Anomalous Currents to an Electrode in a Magnetoplasma

J. M. Urrutia and R. L. Stenzel
Department of Physics, University of California, Los Angeles, California 90024
(Received 31 March 1986)

An electrode pulsed to a large positive potential ($V >> kT_e/e$) in a collisionless magnetoplasma is observed to draw currents far in excess ($10\times$) of the field-aligned electron saturation current prescribed by probe theory. The large currents are inferred to be due to anomalous cross-field transport caused by current-driven instabilities. Electric fields due to space-charge separation and anomalous conductivity lead in time to ion expulsion from the current channel and hence to density depletion and current collapse.

PACS numbers: 52.40.Hf, 52.25.Fi, 52.35.Qz, 52.70.Ds

The current to an electrode biased above the plasma potential in a collisionless plasma is a long-standing problem of fundamental interest in plasma diagnostics[1-3] and current systems in space.[4] Earlier reports[5] have derived the plasma parameters from probe characteristics but have not considered the perturbing effects of saturation currents on the plasma. In this Letter we report measurements of the spatial and temporal evolution of the electron saturation current system, $\mathbf{J}(\mathbf{r},t)$, within the plasma as well as detailed diagnostics of electric field, density, and temperature. From the observations we conclude that electrons drawn by a highly biased ($V >> kT_e/e$), pulsed probe raise the plasma potential in the flux tube roughly subtended by the electrode giving rise to electron Hall currents, expulsion of the unmagnetized ions from the flux tube, and anomalous radial electron currents. The enhanced parallel current near the probe creates an anomalously low parallel conductivity $\sigma(J)^*_{\parallel}$ which results in resistive electric fields, $E_{\parallel} = J_{\parallel}/\sigma(J)^*_{\parallel}$, far outside of the sheath region. Ions are accelerated away from the probe and electrons toward it resulting in a net density depletion, $n_e = n_i \rightarrow 0$, and hence the probe current collapses. Recovery of the current-driven instability causes plasma to flow back to the perturbed region and the process repeats periodically creating pulsating currents in steady state. The large transient current pulses penetrate into the plasma along $\mathbf{B}_0$ at near electron thermal speeds, but since they exist only over durations of ion transit times across the current channel the penetration along $\mathbf{B}_0$ is limited to distances

$$L = \frac{v_{d,e}}{v_{d,i}} r_{ft} \approx \left(\frac{kT_e m_i}{4\pi e \Delta\phi m_e} \right)^{1/2} r_{ft},$$

where $\Delta\phi$ is the radial potential drop in the channel and r_{ft} the flux tube radius. Our plasma is much larger than these scales; hence the results are not boundary dependent and can be scaled to relevant applications.[4]

The experiments are conducted in the quiescent afterglow ($t = 120$ μsec) of the pulsed ($t_{\rm rep} = 2$ sec, $t_{\rm on} = 4$ msec) plasma ($n_e \simeq 2\times10^{11}$ cm^{-3}, $T_e \simeq 5T_i \simeq 1.5$ eV, $B_0 \simeq 30$ G, $p_n \simeq 4\times10^{-4}$ Torr, Ar) schematically shown in Fig. 1(a). The electrode is a tantalum disc of 0.8-cm radius (r_D) insulated on one side. It is biased to $V = 80$ V ($>> kT_e/e$) via a transistor switch with respect to the grid anode and chamber walls. The magnetic field, $\mathbf{B}(\mathbf{r},t)$, induced by the current is measured with a probe consisting of three electrostatically shielded, small (1-cm diam), orthogonal magnetic loops. The probe tip is capable of scanning a suitably large volume ($0 < r < 8$ cm, $0 < z < 55$ cm) about the electrode. The current-density vector field, $\mathbf{J}(\mathbf{r},t)$, is calculated via $\mathbf{J} = \nabla \times \mathbf{B}/\mu_0$. The local plasma parameters (n_e, kT_e, $\phi_{\rm pl}$) are obtained with a small (1×1.5-mm^2) Langmuir probe. The probe tip can also scan a volume about the electrode. The probe bias is changed in successive shots and the probe current-voltage characteristic as a function of time is reconstructed at each spatial point. The acquisition and handling of the necessary large data set is done by computer.[6]

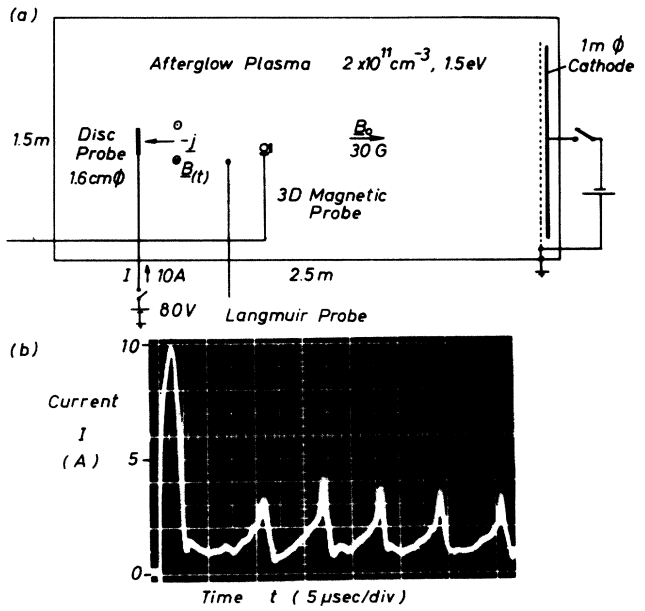

FIG. 1. (a) Experimental device. (b) Electrode current I vs time t at $V = 80$ V.

The normally floating electrode is pulsed (rise time $\simeq 200$ nsec, $t_{on} \geq 40$ μsec) to the supply voltage. The probe current exhibits a temporary increase above the expected electron saturation current ($I_{e,sat} = \pi r_D^2 \times ne[kT_e/2\pi m_e]^{1/2} \simeq 1$ A) whenever the supply voltage exceeds the plasma potential. Current overshoots have earlier been observed[7] and explained theoretically[2,7] by excess ions in the probe sheath but here we will show that the underlying physics is different. After the first current overshoot smaller current peaks appear at somewhat regular time intervals. This implies that no steady-state ($\partial/\partial t \simeq 0$) currents exist, presumably because the plasma has been radically perturbed by the first overshoot. This Letter concentrates on the first overshoot ($I_{max} = 10$ A) caused by an 80-V bias [Fig. 1(b)].

The penetration of currents or magnetic fields is addressed by observation of the temporal evolution of magnetic energy density, $B^2/2\mu_0$, as shown in Fig. 2. The front of the magnetic energy-density perturbation, arbitrarily chosen as the first contour, assumes a speed of $v \simeq 2\times 10^7$ cm/sec, nearly the thermal electron drift speed to the probe, $v_{d,e} = (kT_e/2\pi m_e)^{1/2} \simeq 2\times 10^7$ cm/sec, but lower than the speed of a whistler wave packet of 2-μsec duration,

$$v_g \simeq 2c/\omega_{pe}(\omega\omega_{ce})^{1/2} \simeq 9\times 10^7 \text{ cm/sec},$$

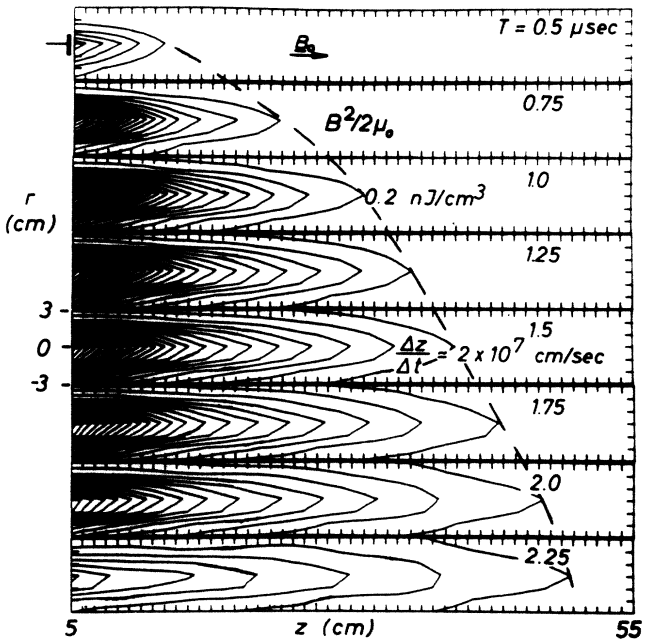

FIG. 2. Contours of constant magnetic energy density in the r-z plane at different times. Contour separation is 0.2 nJ/cm^3. The front asymptotically assumes a speed of 2×10^7 cm/sec. The electrode is shown to scale in the first panel; however, it is located at $z = 0$ cm.

and much faster than the Alfven speed,

$$v_A = B_0/(\mu_0 n m_i)^{1/2} \simeq 3\times 10^6 \text{ cm/sec},$$

and the ion sound speed,

$$c_s = (kT_e/m_i)^{1/2} \simeq 2\times 10^5 \text{ cm/sec}.$$

The region of maximum energy, which is also the region of maximum current density, does not extend far ($z \lesssim 20$ cm) from the electrode. The axial divergence implies that currents are not confined to flow along the flux tube but must funnel radially in from the entire plasma into the electrode.

Examination of the current density reveals the existence of both parallel and perpendicular currents. Figures 3(a) and 3(b) display, for example, the current density ($J_\parallel \lesssim 0.7$ A/cm^2, $J_\perp \lesssim 0.4$ A/cm^2) in the plane $z = 5$ cm at $t = 1.5$ μsec. The direction of $J_\perp$ is mainly azimuthal to the flux tube, i.e., a Hall current, and partly radial outside the flux tube. Consequently,

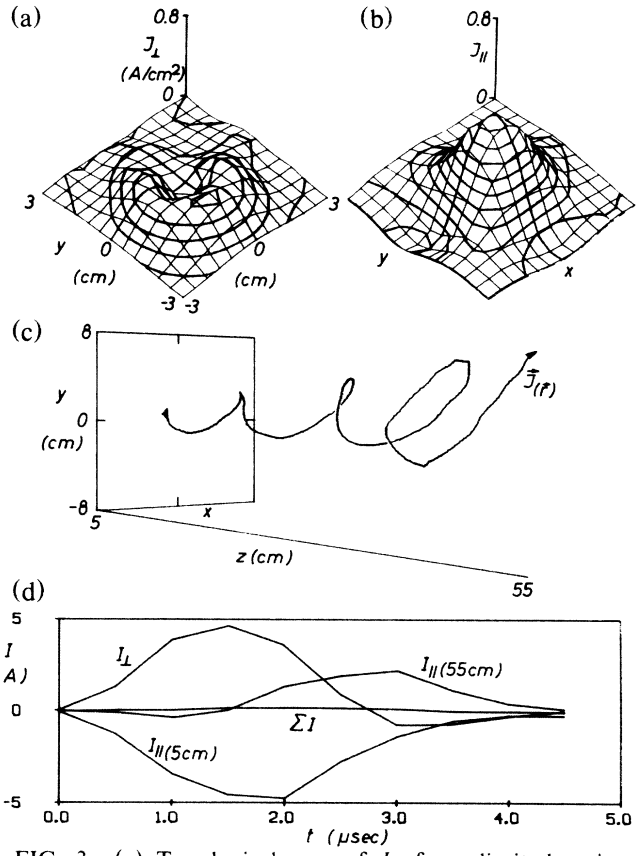

FIG. 3. (a) Topological map of $J_\perp$ for a limited region about the origin for the plane $z = 5$ cm at $t = 1.5$ sec. Contour spacing is 0.08 A/cm^2. Maximum value is 0.8 A/cm^2. (b) Same as (a) but for $J_\parallel$. Maximum value is 0.4 A/cm^2. (c) Trajectory of a current density line at $t = 1.5$ μsec exhibiting the right-handed, conical helix of varying pitch path. (d) Current at the boundaries of the explored volume as a function of time.

the current flows along nested right-handed conical helices whose apex is at the electrode. Because $J_\perp/J_\parallel$ is a function of space, the pitch and conical angle of the helices vary continuously. A typical example out of the infinite set of current-density lines is shown in Fig. 3(c). While the current density describes the local properties of the current system one would also like to know the integrated currents $I = \int \mathbf{J} \cdot d\mathbf{A}$. Figure 3(d) shows that the current across the surface closest to the electrode ($I_{\parallel, z=5\text{ cm}}$) evolves in time as the externally measured current [Fig. 1(b)]. Its magnitude, however, is not the same since it is measured at $z = 5$ cm. Current flowing through the opposite surface ($I_{\parallel, z=55\text{ cm}}$) is initially much smaller than the current at $z = 5$ cm. However, the perpendicular current flowing out of the four side surfaces of the rectangular volume explored [Fig. 3(c)] account for $I_{\parallel, z=5\text{ cm}}$ in spite of the low magnitude of $J_\perp$ on the boundaries. Hence, current is funneled into the electrode. Only after the current overshoot begins to decay does $I_{\parallel, z=55\text{ cm}}$ overtake $I_\perp$ as the source for $I_{\parallel, z=5\text{ cm}}$. The late appearance of flux across the plane at $z = 55$ cm is clearly due to the propagation of the current front. The closure path for the current therefore evolves in time and probably encompasses the entire plasma volume. It is appropriate to note that

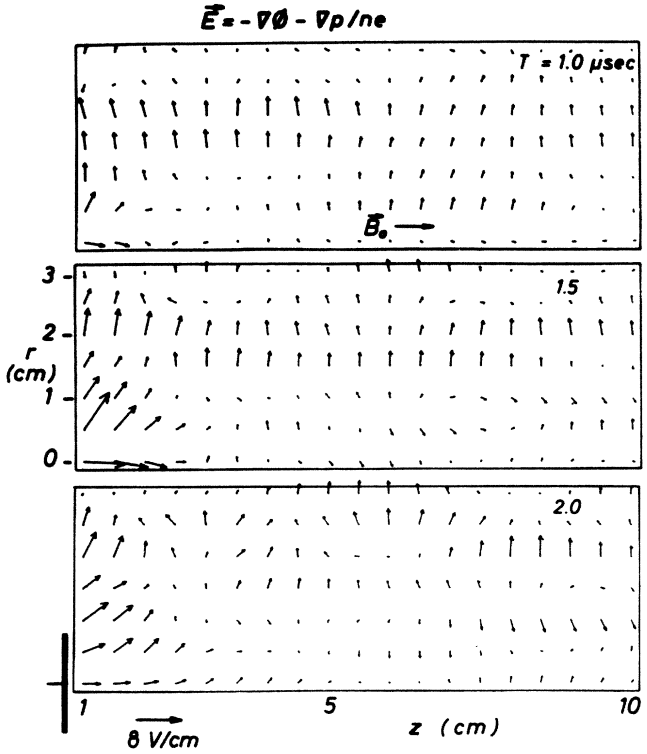

FIG. 4. Vector field map of the net electric field, $\mathbf{E}(\mathbf{r},t) = -\nabla\phi - \nabla_{p/ne}$, for selected times. The electrode is shown to scale in the bottom panel; however, it is at $z = 0$ cm.

$\sum I = \oint \mathbf{J} \cdot d\mathbf{A}$ is not strictly zero at all times ($\approx 5\%$ of $I_\perp$ at $t = 1.5$ μsec) indicating that current measurements may have a similar error.

Upon switchon of the electrode bias, the plasma potential is observed to rise with negligible delay throughout the entire plasma by as much as $\Delta\phi \approx 30$ V and near the probe by $\Delta\phi \approx 40$ V. The global potential shift is caused by the return electrode (grid anode and chamber walls) which must draw an ion current equal to the electrode electron current so as to maintain charge neutrality. The local potential gradients near the electrode are observed to extend well beyond the sheath region [thickness $\delta \simeq (\Delta\phi/kT_e)^{1/2}\lambda_{De} \approx 5\lambda_{De} \simeq 0.15$ mm]. Figure 4 shows vector maps of the net electric field, $\mathbf{E}(\mathbf{r},t) = -\nabla\phi - \nabla(nkT_e)/ne$. Inductive electric fields are negligible compared to the electrostatic fields [$\partial A/\partial t \approx 1$ mV/cm]. One can observe the following features: (a) At early times ($t \simeq 1$ μsec) the electric field is predominantly radial ($E_r \approx 2$ V/cm) as a result of an excess positive charge [$(n_i - n_e)/n_i \approx 10^{-4}$] in the flux tube caused by electron drain to the probe; and (b) as the probe current peaks, an unexpectedly strong parallel field [$E_z \gtrsim 4$ V/cm $>> \nabla(nkT_e)/ne$] builds up near the probe ($z < 3$ cm). The consequence of the radial field is an azimuthal drift of the magnetized electrons ($v_\theta = \mathbf{E}_r \times \mathbf{B}_0/B_0^2 \simeq 6\times10^6$ cm/sec) producing the Hall currents ($J_\theta \approx ne v_\theta \lesssim 0.4$ A/cm^2) and a radial outflow of the unmagnetized ions ($r_{ci} \approx 20$ cm $>> r_{ft} \approx 2$ cm $>> r_{ce} \approx 2$ mm) causing a small radial current density ($J_r = nec_s \approx 5$ mA/cm^2),

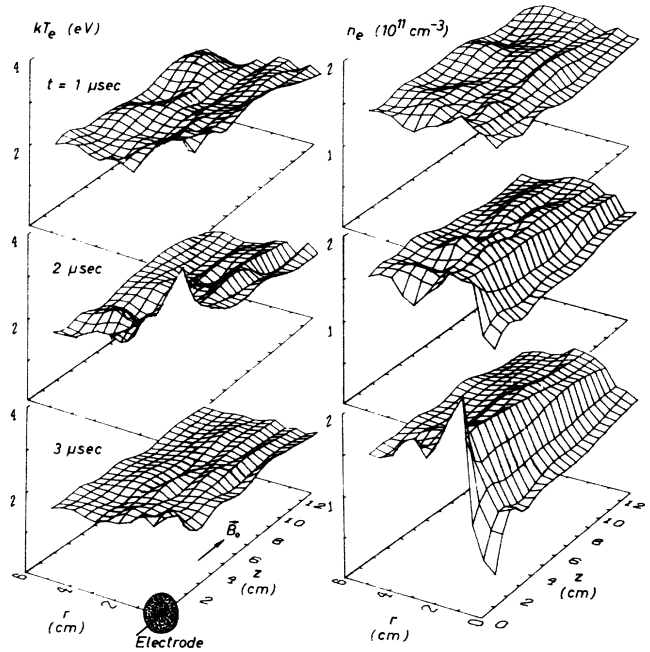

FIG. 5. Space-time dependence of electron temperature, kT_e, and density, n_e.

which when integrated over the large cylindrical area involved yields significant currents ($I_{\perp i} \simeq 2\pi r_{fl} L_{\parallel} J_r \simeq 3.1$ A). The Hall current is expected to generate ion-sound turbulence[8] ($v_\theta >> c_s, T_e >> T_i$) producing azimuthal-wave electric fields, E_θ, and radially inward electron Bohm transport[3] ($I_{\perp e} \gtrsim I_{\perp i}$). Thus the radial transport of ions and electrons accounts for the unexpected cross-field currents. The large parallel electric field produces electron heating [or increase in mean energy if $f_e(\mathbf{v}, \mathbf{r}, t)$ is non-Maxwellian] and acceleration of ions away from the electrode with a resultant density depression. Both of these effects are shown in Fig. 5 which displays kT_e and n vs (r,z) at different times. Local heating is observed during times and locations of strong $\mathbf{E} \cdot \mathbf{J}$ ($t \approx 1.5$ μsec, $z < 3$ cm). The increase in kT_e and the electron-ion drift velocity produces ion acoustic[8] and Buneman[9] instabilities ($v_d \simeq 1.2 \times 10^8$ cm/sec $> v_{th,e} \simeq 7 \times 10^7$ cm/sec $>> c_s$, $T_e >> T_i$) which have been tentatively identified in observed density-fluctuation spectra. Such instabilities produce the anomalous parallel conductivity[10] which, in turn, explains the large parallel electric fields.

In summary, currents far above the electron saturation current can momentarily be collected in a magnetoplasma. Such large currents are due to the appearance of anomalous conductivity and are possible only when the electrode bias is rapidly switched above the plasma potential. The large currents are terminated by the onset of anomalous electric fields which lead to ion expulsion, and hence density depletion, from the vicinity of the electrode. The observations have profound bearing in the use of rapidly swept Langmuir probes, charging of spacecraft, and the proposed shuttle electrodynamic tether system.[4]

The authors are deeply indebted to Dr. W. Gekelman and Mr. L.-Y. Xu for the use of the data acquisition software. The research was supported by National Science Foundation Grants No. PHY84-10495 and No. ATM84-01322, and Air Force Office of Scientific Research Grant No. F19628-85-0003.

[1]H. M. Mott-Smith and I. Langmuir, Phys. Rev. **28**, 724 (1926).

[2]F. F. Chen, in *Plasma Diagnostic Techniques,* edited by R. H. Huddleston and S. Leonard (Academic, New York, 1965), p. 113.

[3]D. Bohm, in *The Characteristics of Electrical Discharges in Magnetic Fields,* edited by A. Guthrie and R. K. Wakerling (McGraw-Hill, New York, 1949), Chaps. 1, 2, and 9.

[4]L. M. Linson, J. Geophys. Res. **74**, 2368 (1969); P. M. Banks, P. R. Williams, and K.-I. Oyama, Planet. Space Sci. **29**, 139 (1981); H. B. Garrett, Rev. Geophys. Space Phys. **19**, 577 (1981); U. Samir, N. H. Stone, and K. H. Wright, Jr., J. Geophys. Res. **91**, 277 (1986).

[5]T. Dote, H. Amemiya, and T. Ichimiya, Jpn. J. Appl. Phys. **3**, 789 (1964); M. Sugawara and Y. Hatta, J. Appl. Phys. **36**, 314 (1965); F. F. Chen, C. Etievant, and D. Mosher, Phys. Fluids **11**, 811 (1968).

[6]W. Gekelman and L.-Y. Xu, Rev. Sci. Instrum. (to be published).

[7]D. G. Bills, R. B. Holt, and B. T. McClure, J. Appl. Phys. **33**, 29 (1962).

[8]D. B. Fried and R. W. Gould, Phys. Fluids **4**, 139 (1961); D. B. Fenneman, M. Raether, and M. Yamada, Phys. Fluids **16**, 871 (1973); R. L. Stenzel and W. Gekelman, Phys. Fluids **21**, 2024 (1978).

[9]O. Bunemann, Phys. Rev. **115**, 503 (1959).

[10]K. Papadopoulos, Rev. Geophys. Space Phys. **15**, 113 (1977).

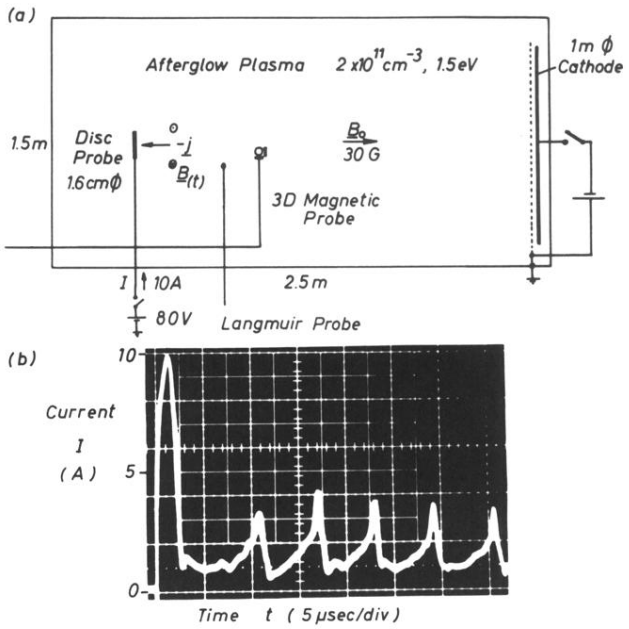

FIG. 1. (a) Experimental device. (b) Electrode current I vs time t at $V = 80$ V.